Nanoscale

PAPER

View Article Online
View Journal | View Issue

Cite this: *Nanoscale*, 2017, **9**, 17378

Compact plasmonic optical biosensors based on nanostructured gradient index lenses integrated into microfluidic cells

A. Horrer, *[a,b] J. Haas,[a,b] K. Freudenberger,[c] G. Gauglitz,[c] D. P. Kern[a,b] and M. Fleischer*[a,b]

Received 8th June 2017,
Accepted 2nd October 2017

DOI: 10.1039/c7nr04097k

rsc.li/nanoscale

We report on a compact and cost-effective integrated label-free biosensor configuration which is based on the refractive index sensitivity of the localized surface plasmon resonance (LSPR) of gold nanostructures. Aiming for compactification and miniaturization of the sensor, arrays of nanodiscs were fabricated on the planar surface of a gradient index (GRIN) lens, which acts as a substrate as well as an imaging objective for the light scattered by the gold structures. Integration of the lens into a microfluidic flow cell enabled the controlled exchange of liquid media at the sensor surface. The light scattered by the nanostructures was investigated spatially and spectrally resolved making use of the imaging properties of the GRIN lens. Dynamic spectral analysis during refractive index changes was conducted, revealing high sensitivities of up to 372 nm per refractive index unit for the shift of the LSPR. Biosensing capabilities were demonstrated by the detection of binding of an analyte by means of a testosterone-immunoassay.

Introduction

For many practical applications such as medical diagnosis, environmental surveillance, or food quality monitoring, compact, portable and inexpensive setups for sensing of molecules are beneficial and are becoming more and more important. Label-free sensing techniques provide high potential for this kind of application.[1]

One example for such techniques is the application of metallic nanostructures and their optical properties, which are sensitive to refractive index changes in their close vicinity. The light scattered by metallic nanostructures under illumination exhibits resonances in its spectrum. These resonances occur due to the excitation of collective oscillations of the conduction electrons in the nanostructure, so-called localized surface plasmon resonances (LSPRs), whose spectral positions depend on the structures' material, size and shape, and the dielectric properties of their surrounding medium.[2–5] The spectral dependency of the resonances on refractive index changes in their close vicinity has been widely used in applications such as biosensing.[6–11] In many cases an immunoassay is used, for which the nanostructures are functionalized with specific recognition structures for the detection of a certain analyte from solution.[12–15] A related label-free refractive index sensing method is based on the surface plasmon resonance (SPR) of, typically, thin gold films.[16] This technique is widely used and commercially available. A way to increase the applicability of biosensors is the ability for multiplexing on a single compact chip, which requires appropriate spatial resolution. For SPR chips this can be achieved by selective functionalization of different areas and performing SPR imaging.[17] While this is also possible for LSPR sensing, it has the added advantage of very good spatial resolution due to the small sizes of its sensing elements, providing a means for multi-parameter sensing by evaluating individual structures or small assemblies in parallel. However, this requires the ability to read the elements out separately. A common way to image plasmonic nanostructures and to examine their scattering spectra with high resolution is dark-field microscopy and spectroscopy.[18] In a dark-field microscope the sample, *e.g.* a microscope slide with metallic nanoparticles on its surface, is illuminated with white light incident under a large angle which ensures that the numerical aperture (NA) of the illuminating light is larger than the NA of the detecting objective. That way only light scattered by the structures in the forward direction is collected and can be examined with down to single particle resolution.

The use of the optical properties of metallic nanostructures offers easy optical read-out with light in the far-field modified

[a]*Institute for Applied Physics, University of Tübingen, Auf der Morgenstelle 10, 72076 Tübingen, Germany. E-mail: andreas.horrer@uni-tuebingen.de, monika.fleischer@uni-tuebingen.de*
[b]*Center for Light-Matter-Interaction, Sensors and Analytics LISA+, University of Tübingen, Auf der Morgenstelle 15, 72076 Tübingen, Germany*
[c]*Institute for Physical and Theoretical Chemistry, University of Tübingen, Auf der Morgenstelle 18, 72076 Tübingen, Germany*

by effects in the near-field of the structures without having to interfere directly with the measurement system. Typically this takes place in a microscope as described above. In this work a step towards compactification is pursued by making use of the substrate that the structures are fabricated on as part of the imaging system. Gradient index (GRIN) lenses are very suitable for this approach. GRIN lenses achieve their focusing properties by a spatially varying internal refractive index.[19] Compared to conventional lenses their prominent advantages for the implementation as a biosensor substrate are their planar surfaces, and the possibility to have their focal plane located directly on one of these surfaces. The planar surfaces enable controlled placement of metallic nanostructures on the lens, which then can be directly imaged, using the GRIN lens as an objective, since they automatically are in focus. Compared to standard microscope objectives, this configuration is much more compact, since GRIN lenses have diameters of only few millimeters, and no space between the objective and sensor surface is required. Furthermore, no focusing routines have to be performed before each sensing measurement, which enables straightforward operation and an increased throughput. GRIN-terminated glass fibres have found their application in miniaturized endoscopy, *e.g.* for eye surgery, for few decades now.[20,21] The possibility to build small-volume optical elements based on GRIN lenses plays an important role in the development of non-invasive and flexible microscopy techniques *e.g.* for *in vivo* investigations.[22] Using a GRIN lens system on an endoscopic head, miniaturized confocal laser scanning microscopy suitable for diagnostic endoscopy was developed.[23] GRIN-lenses have expanded the capabilities of intravital fluorescence microscopy as well as two-photon microscopy.[24–26] For improved (sub-wavelength) resolution, GRIN lenses were recently decorated with microspheres.[27] The GRIN lenses can be further miniaturized by creating nanostructured gradients *via* a combination of subwavelength sized glass rods of different indices.[28] A GRIN lens can be characterized by few parameters. The refractive index profile, which is defined by the gradient constant g, determines how light is refracted inside the lens and therefore defines the light path through the lens. For a cylindrical lens the refractive index is a function of the radial position r. If the profile can be approximated by a parabola with its maximum n_0 in the center of the cylinder ($n(r) = n_0 \times (1 - g^2r^2)$), it results in a cosine ray trace within the lens, when illuminated by collimated light through one of the planar surfaces (see Fig. 1). This desirable profile can be realized by diffusion of ions as impurities into the glass. Another parameter of the lens is the pitch, which is its length divided by the period of the cosine ray trace. By changing the length and thereby the pitch, the focal plane of the lens can be set to the desired distance from the surface of the lens, including directly on the surface for odd multiples of 1/4 pitch.

By adjusting these parameters a GRIN lens can be fabricated such that its focal plane is located directly on its planar surface when illuminated with collimated light. Structures on this surface can be imaged through the lens. By simplifying

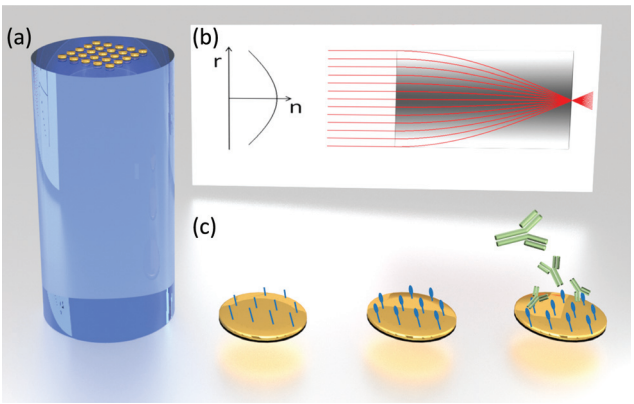

Fig. 1 (a) Schematic of a GRIN lens with a nanostructure array on its flat surface, (b) radial refractive index profile $n(r)$ and ray path in a quarter-pitch GRIN lens, and (c) schematic of an immunoassay on a gold nanodisc.

the radiation of plasmonic nanostructures to that of a point light source, one can assume that the light originating from such structures will leave the GRIN lens as parallel beams. Placing the structures on the surface of a GRIN lens thus obviates the need for an objective in a microscope. The parallel light leaving the lens can either be coupled into the remaining optics of a microscope (tube lens and eyepiece or camera) for imaging or be directly investigated spectrally by coupling to a spectrometer. These possibilities can pave the way for inexpensive and miniaturized optical setups for the spectroscopy of plasmonic nanoparticles, which are needed in *e.g.* biochemical or medical sensing devices.

In this work gold nanodiscs were fabricated on the surface of GRIN lenses. The nanostructured lens, after integration in a microfluidic system, was used as a compact sensing platform. The scattered light of the structures under illumination with white light was collected to image the nanostructures by using the GRIN lens as an objective in a microscope. Furthermore, connecting the nanostructured GRIN lens to a spectrometer enabled the investigation of the structures' LSPRs. The microfluidic flow cell allowed demonstrating the sensor functionality of the system by investigating refractive index changes caused by changing the fluids in contact with the lens surface. A biosensing feasibility study was conducted using an immunoassay to detect the interaction between testosterone and anti-testosterone antibodies.

Materials and methods

Nanostructured GRIN lens

The GRIN lenses were purchased from GoFoton and are made of glass, with a gradient index prepared by ion exchange, resulting in an inhomogeneous distribution of impurities.[29] One of the key advantages is their compact size. The lenses used in this work had a length of 10.24 mm and diameter of 4 mm. However, direct processing of small surfaces on a 3D

structure like the GRIN lens with standard electron beam lithography is challenging, since homogeneous resist layers are required. Therefore a transfer process was adapted following ref. 30 to prepare plasmonic structures on the surface of a GRIN lens. Fig. 2(a) shows the process steps schematically. Gold nanodiscs were fabricated on a silicon wafer by electron beam lithography (EBL), deposition of a 30 nm gold film by thermal evaporation, and lift-off in acetone in a first step. This enabled a controlled process and allowed to check the structure dimensions by scanning electron microscopy (SEM) after fabrication. For the sensing experiments large arrays of near-identical structures were fabricated, the dimensions of which can be seen in Fig. 2(b). Two examples of nanodiscs with diameters of about 80 nm and 150 nm are shown. The structures chosen for the experiments described later had similar diameters. They were adjusted for their resonances to occur at around 640 nm and 840 nm, respectively, when they are located on a GRIN lens surface in a water environment to enable a comparison of their size-dependent sensitivities. For imaging experiments, additionally a series of test structures consisting of stripes with varying widths and circles with varying diameters from 2.5 μm down to 250 nm were fabricated repeatedly with distances of 100 μm across a length of 4 mm in order to cover the whole diameter of a GRIN lens. In the second step the transfer process was applied to move the structures from one substrate to another. For this process a transfer material with a favorable surface energy is required, to which the structures adhere more strongly than to the substrate they are initially fabricated on. Therefore, a mixed polymer was used, which contains a component for chemical bonding to the gold structures *via* thiol groups. The polymer was prepared in solution to be able to apply a thin film to the sample. It consists of pentaerythritol tetrakis (3-mercaptopropionate) (Sigma Aldrich), di(trimethylolpropane) tetraacrylate (Sigma Aldrich) and the photoinitiator Irgacure 754 (Ciba AG) solved in propylene glycol methyl ether acetate (Sigma Aldrich). The surface of the wafer with the nanostructures was spin-coated with the prepolymer solution to achieve a homogeneous layer thickness of a few micrometers. A thin polydimethylsiloxane (PDMS) sheet, which acts as the carrier for the thin polymer layer for the transfer, was lightly pressed onto the prepolymer. The prepolymer was then cured by UV-light for 10 min. The silicon wafer with the nanostructures, the cured polymer and the PDMS now formed a solid compound. After immersion in water for two hours to promote dissociation of the polymer and silicon, the PDMS and the polymer could be peeled off the silicon wafer, leaving the gold structures bonded to the polymer. The gold structures were then transferred by lightly pressing the assembly onto the surface of a GRIN lens and heating for 20 min at 70 °C to promote adhesion. Eventually the PDMS sheet was peeled off to leave the polymer and nanostructures on the GRIN lens. The polymer was removed using oxygen plasma to uncover the gold structures. In Fig. 2(c) an optical image of a final nanostructured GRIN flat with a 500 × 500 μm^2 square array of similar discs with a period of 500 nm can be seen. It consists of 15 × 15 square arrays with sizes of 25 × 25 μm^2, which can be distinguished in the optical images. This field size was chosen due to the specifications of the electron beam exposure system. Each of the writing fields contains an array of nanodiscs as shown in Fig. 2(b) that can only be clearly resolved in SEM images. Fig. 2(d) shows a test structure of bars and circles with sizes ranging from 2.5 μm down to 250 nm, which were completely transferred to the surface of a GRIN lens. The structure was imaged through the different stages of fabrication. The SEM image on the left shows the structures after EBL on a silicon wafer. In the center a dark-field microscopy image of the structures after embedding in the transfer polymer and stripping off the silicon can be seen. The image on the right shows the structures after the completed transfer on a GRIN lens. The structures are imaged using the GRIN lens as an objective as described later, with the corresponding image quality of this cost-effective optical element.

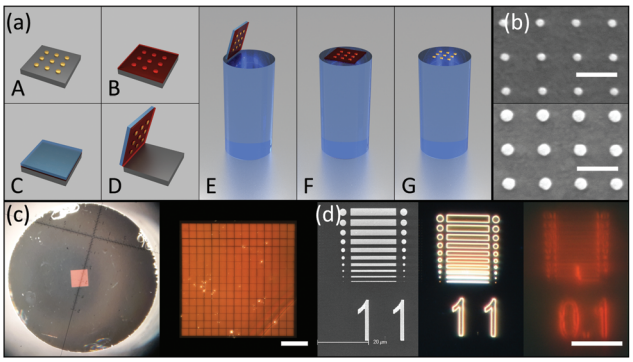

Fig. 2 (a) Schematic of the steps for the fabrication of gold nanostructures on the surface of a GRIN lens by transfer: A: electron beam lithography of gold nanodisc arrays on Si, B: embedding in prepolymer, C: add PDMS sheet, D: remove disks from Si surface by peeling off PDMS, E: transfer to GRIN lens, F: removal of PDMS sheet, G: removal of polymer, (b) SEM images of exemplary nanodisc arrays on Si (scale bars are 500 nm), (c) optical images of a nanostructure array on the flat surface (diameter 4 mm) of a GRIN lens (scale bar 100 μm), and (d) SEM image of test structures on Si substrate, dark-field microscopy image after transfer to a PDMS stamp, and image through the GRIN lens of the structures on the GRIN surface after complete transfer (scale bar 20 μm).

The integrity of the morphological and optical properties of the gold nanodiscs throughout the transfer process was further monitored by performing transfers onto glass cover slides. In Fig. 3(a), part of an array of 140 nm diameter nanodiscs with 350 nm spacing can be seen after fabrication on a silicon substrate. In Fig. 3(b), the array is shown after transfer to the glass substrate. The insulating surface was sputter-coated for imaging purposes. The structures appear intact, with comparable sizes and spacing as before. In Fig. 3(c), dark-field transmission spectra of a nanodisc array are shown throughout the different steps of the transfer. The spectra are recorded in a Nikon Eclipse TI-U inverted microscope with a 20× objective (NA 0.5) and an Ocean Optics QE65000 spectrometer, and normalized to the lamp spectrum. The blue

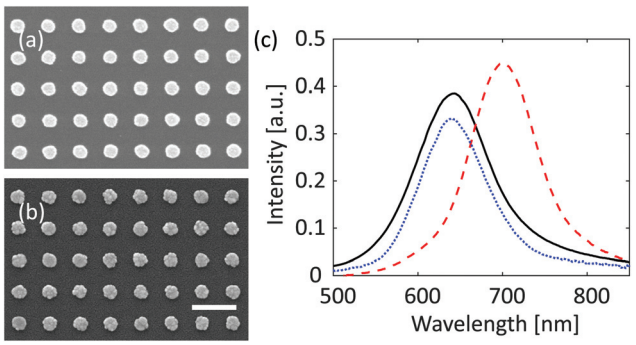

Fig. 3 (a) SEM image of part of an array of nanodiscs with diameters of 140 nm and a period of 350 nm on a silicon substrate, (b) SEM image of the nanodisc array after transfer to a cover glass (the surface was sputter-coated due to the insulating glass substrate, scale bar is 500 nm), and (c) sample dark-field spectra of a nanodisc array after embedding the nanodiscs in polymer and peeling them off the silicon surface (blue dotted line), placing the polymer with the nanostructures on the glass substrate (red dashed line), and the nanodiscs on the glass substrate after removing the polymer (black solid line).

(dotted) curve shows the nanodiscs resonance after embedding the structures into the polymer and peeling them off the silicon. The refractive index of the polymer is similar to that of glass. The red (dashed) curve shows the particle resonance after the nanodiscs on polymer are placed on the glass substrate. At this stage they are surrounded by a high-index medium, which leads to a shift of the resonance to longer wavelengths. The black (solid) curve shows the resonance of the nanodiscs on glass after the polymer is removed. The spectral shape and resonance wavelength are maintained throughout the transfer.

With some experience, the transfer process proved to be highly reliable. Out of the $>5 \times 10^5$ nanodiscs that were transferred for each GRIN lens only a few structures were missing, as can be seen from the homogeneity of the dark-field overview images (*e.g.* Fig. 2(c)). Most remaining defects already resulted from the lift-off after the nanostructure fabrication on the silicon wafer, which was due to the intentional lack of an adhesion layer, rather than from the transfer. This process can be employed more generally to fabricate structures on surfaces that are difficult to handle by standard techniques, such as non-conducting, very small or curved substrates. Another advantage of this process compared to the direct fabrication on glass substrates is that the structures can be characterized by SEM before the transfer to measure their size and shape, since they can be fabricated on a conducting substrate. This would be more difficult for structures prepared directly on a GRIN lens surface. Furthermore the optical spectra of the structures can be compared between the different stages of the transfer process as shown in Fig. 3(c).

Microfluidic cell

For refractive index sensing experiments a flow cell with a microfluidic channel was fabricated to allow for the controlled exchange of different liquid media at the sensor surface.[31] A commonly used material is PDMS, which can easily be molded into various shapes. The resulting flow cell can thus be adjusted to the requirements of the experimental setup. The integration into a microfluidic cell is shown schematically in Fig. 4. In a first step, a 100 μm wide and 60 μm high ridge of SU-8 negative photoresist (Microchem) was fabricated on a silicon wafer by optical lithography. The ridge had a length of 1 cm and an annular extension in the middle and served as the negative of a microfluidic channel. Then a GRIN lens was placed on the broadened central ring of the SU-8 channel mold with the nanostructured surface facing the channel. This ensured that the center of the lens surface formed part of the channel, and the structures were not harmed in the further molding process. Additionally, thin metal wires were placed at the ends of the channel mold to serve as a mold for the feed lines to the tubes. Next, the negative microfluidic channel including the feed lines was molded by pouring PDMS into a cylindrical mold. After hardening the PDMS by heating to 100 °C on a hotplate for 1 h, the metal wires and Si/SU-8 mold were carefully removed, and the thus-formed channel was sealed by a microscope coverslip. The PDMS block now monolithically combines the GRIN lens with the structures located in a microfluidic channel as a compact unit.

Sensing surface functionalization

To detect testosterone antibody from solution, the surface of the gold structures was functionalized with testosterone as the recognition element to promote specific binding and suppress non-specific binding in a similar way as described before.[32] For this purpose, in a first step 6-amino-1-hexanethiol hydrochloride, which acts as a linker molecule, was bound to the gold structures *via* its thiol groups forming a self-assembled monolayer. The molecules were therefore dissolved in ethanol with a concentration of 0.84 mg mL^{-1}, and 5 mL of the solution were slowly pumped through a flow cell containing a GRIN lens with nanodiscs with a rate of 7 μL min^{-1} over a

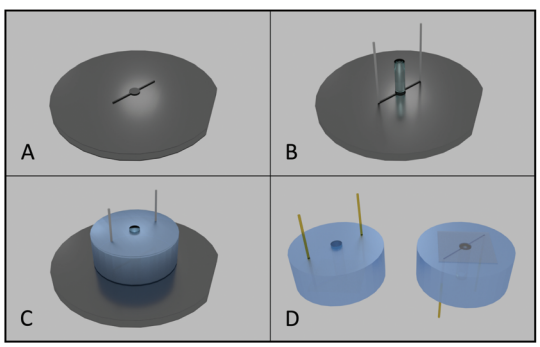

Fig. 4 Schematic of the molding process of the microfluidic cell with integrated nanostructured GRIN lens: A: fabrication of a negative of the microfluidic channel by SU-8 lithography on Si; B: addition of down-facing nanostructured GRIN lens and wires to define the inlet and outlet; C: PDMS-shaping of the fluidic cell; D: final structure after removing the Si with channel mold, closing the channel with a cover slide, and adding tubes for the inlet and outlet (top and bottom views).

period of 12 hours. For the second step a solution containing testosterone 3-(*O*-carboxymethyl)oxime (0.1 g L^{-1}), 1-ethyl-3-(3-dimethylaminopropyl)carbodiimide (20 g L^{-1}) and *N*-hydroxysuccinimide (6 g L^{-1}) in a buffer prepared with 2-(*N*-morpholino)ethanesulfonic acid in water (50 mM, pH 6) was pumped through the flow cell over a period of 20 minutes. This resulted in a covalent binding of the testosterone to the amino group of the aminohexanethiol. With this recognition structure the sensing surface was completed. A schematic of the functionalization and immunoassay procedure is shown in Fig. 1(c).

Results and discussion

Optical imaging and spectroscopy

Depending on the configuration, the GRIN lens can be employed directly for the spectroscopy or microscopy of the nanostructures on the flat surface. The surface of the lens with the nanodiscs is illuminated by white light incident at a high angle. The angle is chosen to be larger than the numerical aperture of the lens. This ensures that the illumination light does not contribute to the intensity detected within an opening angle of 30° on the other side of the lens. In the presented experiments a dark-field condenser with an NA between 0.80 and 0.95 was used. The light scattered by the nanostructures in the forward direction enters the lens and is refracted gradually through the internal index gradient. If for simplicity a scattering nanostructure is approximated as a point light source on the surface of a quarter pitch GRIN lens, the light leaves the lens on the opposing surface as a collimated beam. In the present work the light was coupled into an infinity corrected microscope, such that an intermediate image of the lens surface was formed by the microscope's tube lens. This image was either recorded by a camera or coupled into a spectrometer for LSPR sensing. In the latter case a small area of the beam was cut out by a pinhole with a diameter of 200 μm, which restricted the evaluated image area on the GRIN lens to few microns. The light going through the pinhole was collimated by a lens and coupled to the spectrometer by focusing on its entrance slit *via* another lens. The optical path is schematically illustrated in Fig. 5. Since the illuminating light does not contribute to the parallel beam leaving the lens, the structures on the lens surface are investigated in a setup similar to dark-field microscopy. In Fig. 6(a) an overview image over many arrays of gold nanostructures which are positioned in the center of the lens surface (see Fig. 2(c)) is imaged through the GRIN lens. Such large arrays of similar structures were used for the refractive index sensing experiments shown in the next section. The exit angle of the beam depends on the radial position of the nanostructure on the surface. Reciprocally, collimated light entering the lens under different angles is focused on different spots on the lens surface. The beam paths were simulated with COMSOL Multiphysics using the parameters for the lenses used in the experiments. The results for two different angles can be seen in Fig. 6(b). Therefore tilting the lens by different angles enables imaging of different areas on its surface. A typical NA for a GRIN lens is in the range of 0.5, which means that the maximum angle corresponds to 30°. The resolution limit of such a GRIN lens is therefore in the range of 1.22λ (*i.e.* ~800 nm for long-wavelength visible light).

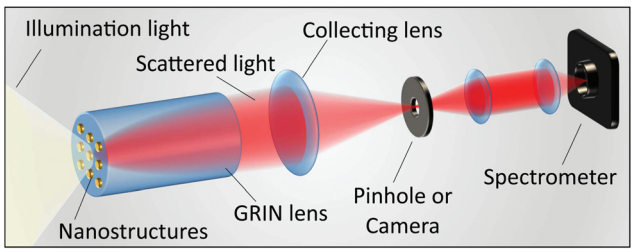

Fig. 5 Optical configuration of the nanostructured GRIN lens for imaging or spectroscopy.

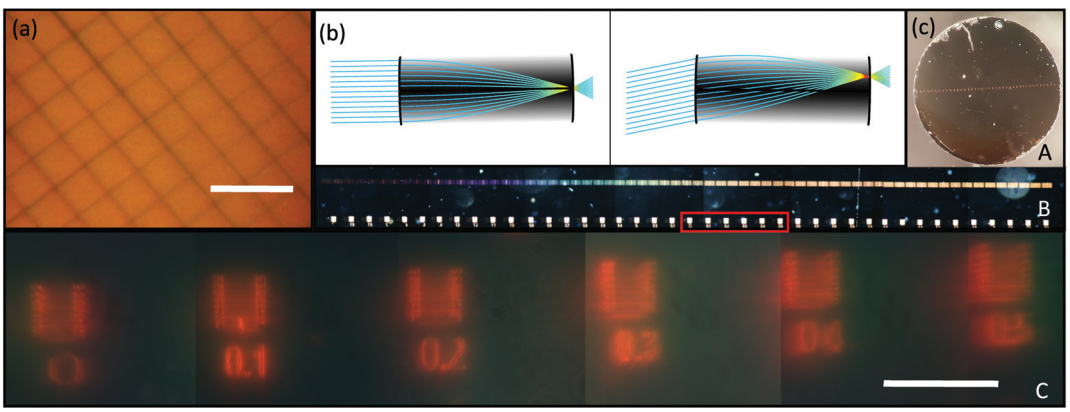

Fig. 6 (a) Arrangement of (25 μm)^2 arrays of gold nanostructures (see Fig. 2(c)) imaged through a GRIN lens (scale bar is 50 μm), (b) ray paths starting at different surface positions passing through a GRIN lens under different angles, (c) images of test structures and markers at different positions on the surface of a GRIN lens imaged (A) as optical overview image over the lens surface (4 mm diameter), (B) in a dark-field microscope and (C) through the GRIN lens by using different beam angles (scale bar is 50 μm).

Fig. 6(c) shows an optical image of the surface of a GRIN lens with different structures spread across its whole diameter that are visible as bright dots (A). Below, the structures are imaged using a dark-field microscope objective (B). The area that is indicated by a red rectangle, which marks structures located up to half a millimeter away from the center, is shown as imaged through the GRIN lens (C). The image is an assembly of several single frames which were obtained by mapping the lens surface by tilting the lens with respect to the camera. Therefore, the lens was attached to a mounting which could be rotated to defined angles.

At multiples of 100 μm distance from the center of the lens surface, lines with decreasing widths and circles with decreasing diameters were prepared to indicate the resolution limit of the lens. The numbers that can be discerned mark the distance from the center in millimeters. This image series proves that it is possible to image different areas on the surface separately, albeit naturally with a lower image quality than with high-end objectives. The light intensity transmitted by scattering is sufficiently high for spectral analysis of the nanostructure resonances. Different areas on the surface can thus be read out simultaneously by collecting the light leaving the lens under different angles. In future work further compactification of the sensing setup can be achieved by omitting the pinhole in Fig. 5 and coupling the collimated light leaving the GRIN lens directly to the spectrometer, while the spatial resolution of the spectral analysis is achieved by evaluating different exit angles. Combined with advanced flow cells with multiple chambers[33] and different specific recognition structures, this would allow for parallel investigation of several immunoassays and detection of different analytes in a compact setup.

According to the manufacturer the refractive index of the lens in the center is n_0 = 1.64. Assuming a parabolic index profile as indicated in Fig. 1 with the parameters taken from the manufacturer, a refractive index of n = 1.56 is found at the edge of the lens surface. This variation of the substrate index affects the resonance wavelengths of nanodiscs located at different radial positions, resulting in a resonance shift in the range of about 14 nm to 20 nm of identical discs between the center and the edge, depending on the disc size. This was determined by simulations of discs with a height of 30 nm and diameters of 80 nm or 150 nm, respectively, on the lens and in a water environment (not shown here). As mentioned above, for the index sensing experiments shown in the next section only discs from an area of a few microns around the center of the lens contributed to the measured spectra. Therefore, the influence of the substrate can be neglected in these measurements, but it has to be taken into account when extending the investigated area to different spots of the lens surface.

Index sensing

The nanostructured GRIN lens was integrated into a microfluidic channel, which was fabricated from PDMS as described above. This way it was possible to immerse the surface and thereby the structures into liquid media with different refractive indices in a controlled way to investigate the resonance shifts of the structures. The lens in the flow cell was illuminated by white light through a dark-field condenser in an inverted microscope as shown schematically in Fig. 5.

For testing the sensitivity of the sensing surface different liquids with varying refractive indices were introduced to the flow cell. By using mixtures of water and glycerol, the refractive indices were adjusted to increase in steps of 0.01 from water with n = 1.33 to 37 wt% glycerol in water with n = 1.38. Each water/glycerol mixture was pumped through the cell for several minutes, followed by pure water to return to the base level and test the stability of the sensor surface. A spectrum was recorded every 10 s, and the resonance peaks in the spectra were fitted with a Gaussian, the maximum of which was plotted over time. The two investigated lenses exhibited resonances at different spectral positions. Because of their different disc diameters, the nanostructures on the two lenses were resonant at wavelengths of about 640 nm and 840 nm, respectively, in water. This has a strong effect on the sensitivity of the structures, since resonances that occur at longer wavelengths have been shown to exhibit larger wavelength shifts per refractive index unit (RIU).[34] The time-dependent fitted resonance wavelength at which the maximum for the larger structures occurs can be seen in Fig. 7(a). The inset shows the shifts of the intensity peak of the GRIN sensor with the resonance at the shorter wavelength. The influence of the different values of the refractive index of the solutions in the flow cell is clearly visible as plateaus of the resonance at different wavelengths. The baseline for water and the plateaus for the different solutions were fitted with straight lines. The distances between the line fits were used as the values for the resonance shifts. Fig. 7(b) shows the shifts per refractive index change in the present two cases. The values were fitted linearly with a least-squares fit, the slopes of which reveal the sensitivity of the sensor surfaces. They result in 139 nm RIU^{-1} for the shorter and 372 nm RIU^{-1} for the longer wavelength resonance. This is in the range of previously reported values for similar plasmonic structures.[35] A lower limit for the detection of refractive index changes can be determined by evaluating the noise in the measurements, which is distinctly below 1 nm, indicated by the area between the red lines in Fig. 7(a) and the dashed line in Fig. 7(b). Hence it should be possible to detect refractive index changes as small as a few ‰ of a RIU. These experiments show that the sensor, consisting of a microfluidics-integrated nanostructured GRIN lens, is very suitable for the detection of even small refractive index changes.

Molecular sensing

The application of the nanostructured GRIN lenses as biosensors was tested with a biological system. As a proof of principle, an immunoassay for testosterone was selected. The interaction of testosterone, immobilized on the sensor surface, with testosterone antibody in solution was detected by evaluating the plasmonic resonance shifts when exposed to analyte solution over time. Following the application of the reco-

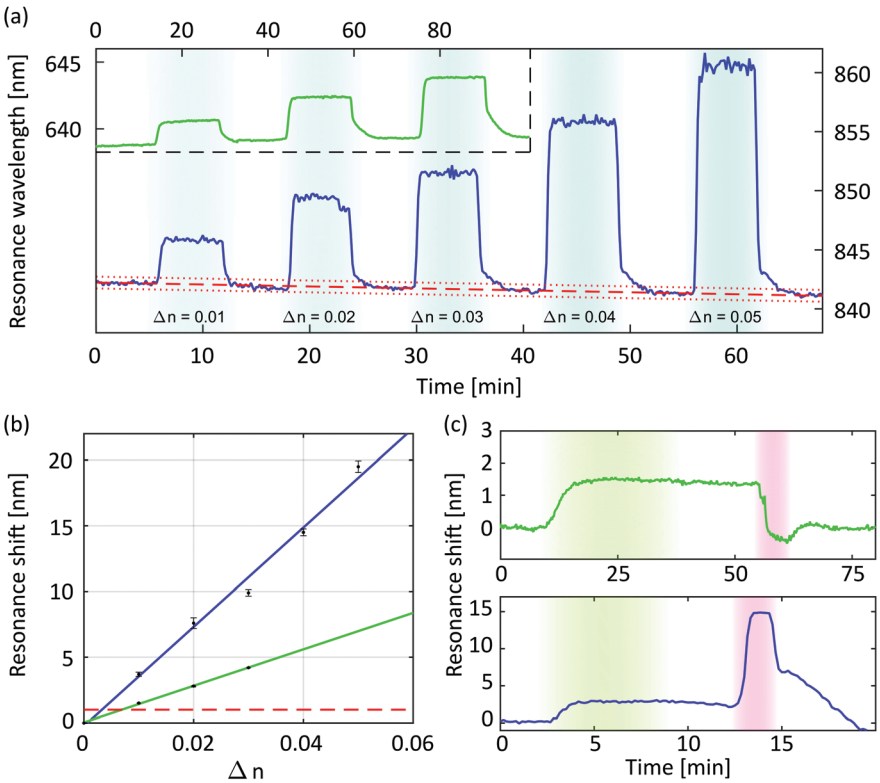

Fig. 7 (a) Shift of the resonance wavelength plotted over time for immersion in media with different refractive indices for two different sensors, (b) resonance shifts *vs.* refractive index change with linear fits, where the slopes correspond to the sensitivities, with the red dashed line indicating the detection limit due to noise, and (c) testosterone immunoassays for the detection of testosterone antibody binding from solution (green areas), using regeneration solutions with different refractive indices (red areas).

gnition structure, as described in the Materials and methods section, the flow cell was mounted onto a dark-field microscope with the GRIN lens acting as the objective as shown before, and solutions with a fixed concentration of 20 mg L^{-1} of anti-testosterone antibody in phosphate-buffered saline (PBS) were pumped over the surface. Fig. 7(c) shows exemplary cycles of buffer flow, antibody binding and regeneration for both sensor surfaces. In both cases a resonance shift caused by adsorbed anti-testosterone molecules was observed. At first PBS (10 mM, pH 7.4) was pumped through the flow cell for some time to obtain a baseline. After an initial regeneration of the surface to remove residues of reagents from the functionalization process (not shown), an antibody solution was pumped through the cell (marked by the green area in the figure). A clear resonance shift with a maximum value of about 1.6 nm for the lens with the smaller discs and 3.4 nm for the lens with the larger discs, which is reached after slowly increasing for several minutes, can be observed. The rising time is characteristic of the binding kinetics. As expected from the experiments before, the shift was stronger for the lens with the longer wavelength resonance due to its higher sensitivity. The resonance wavelength remained at the shifted value for a subsequent step of PBS flow, which indicated stable binding of the antibody to the recognition structure. The surface was afterwards regenerated with solutions of either sodium dodecyl sulfate in the case of the shorter resonance wavelength, or guanidinium chloride for the longer wavelength sensor (shaded in red in the figure). This appears as a blue- or redshift of the resonance wavelength depending on the refractive index of the regeneration solution compared to that of the buffer. After the regeneration the resonance wavelength returned to the initial value. The presence of the testosterone antibody is thus successfully detected with the compact nanostructured GRIN sensor cell. For future optimization, the long-term stability of the recognition structure under repeated regeneration and of the fluidic cell needs to be further improved. Besides the refractive index sensitivity of the nanostructures, in molecular sensing the absolute sensitivity of the biosensor is determined by the diffusion rate of the analyte in the solution towards the nanostructures. For further improvement of the sensor an approach based on transport by dielectrophoresis[36] may be applied.

Conclusions

In conclusion we fabricated a compact biosensor making use of the localized surface plasmon resonances of gold nanostructures on the flat surface of a GRIN lens. The nanostructures can be imaged through the lens, such that the sub-

strate takes the role of the imaging objective. Examining the sample under different angles makes it possible to address structures located in different areas of the surface. The nanostructured lens was implemented in the microfluidic channel of a flow cell and used as an LSPR refractive index sensor. By including the lens into the sensing unit, no bulky and expensive microscope objectives are required for the read-out, and the system forms a compact unit. Refractive index changes down to less than 0.01 could be detected, which shows a suitable sensitivity for the sensing of biomolecules. This was shown exemplarily for a testosterone immunoassay. In future, multiplexing could be achieved by selective functionalization of different sample areas with different recognition structures and employing each such area to detect different analytes. The miniaturized sensing setup and the suitability for sensing small refractive index changes make the nanostructured GRIN sensor cell attractive for flexible, mobile biosensing or medical applications.

Conflicts of interest

There are no conflicts to declare.

Acknowledgements

This work was financially supported by the Baden-Württemberg Foundation as part of the project GRIN-SEN in the research program Optical Technologies. This project was performed in the framework of the European Cooperation in Science and Technology COST Action MP1302 Nanospectroscopy. The authors thank the partners in the GRIN-SEN project for fruitful discussions.

References

1 E. di Fabrizio, S. Schlücker, J. Wenger, R. Regmi, H. Rigneault, G. Calafiore, M. West, S. Cabrini, M. Fleischer, N. van Hulst, M. F. Garcia-Parajo, A. Pucci, D. Cojoc, C. A. E. Hauser and M. Ni, *J. Opt.*, 2016, **18**, 063003.
2 E. Ringe, J. M. McMahon, K. Sohn, C. Cobley, Y. Xia, J. Huang, G. C. Schatz, L. D. Marks and R. P. Van Duyne, *J. Phys. Chem. C*, 2010, **114**, 12511–12516.
3 H. Chen, X. Kou, Z. Yang, W. Ni and J. Wang, *Langmuir*, 2008, **24**, 5233–5237.
4 M. M. Miller and A. A. Lazarides, *J. Opt. A: Pure Appl. Opt.*, 2006, **8**, S239.
5 P. K. Jain, K. S. Lee, I. H. El-Sayed and M. A. El-Sayed, *J. Phys. Chem. B*, 2006, **110**, 7238–7248.
6 A. J. Haes and R. P. Van Duyne, *J. Am. Chem. Soc.*, 2002, **124**, 10596–10604.
7 K. A. Willets and R. P. Van Duyne, *Annu. Rev. Phys. Chem.*, 2007, **58**, 267–297.
8 K. M. Mayer and J. H. Hafner, *Chem. Rev.*, 2011, **111**, 3828–3857.
9 H. Jiang, T. Li, E. Ertorer, J. Yang, J. Sabarinathan and S. Mittler, *Sens. Actuators, A*, 2013, **189**, 474–480.
10 S. S. Acimovic, M. A. Ortega, V. Sanz, J. Berthelot, J. L. Garcia-Cordero, J. Renger, S. J. Maerkl, M. P. Kreuzer and R. Quidant, *Nano Lett.*, 2014, **14**, 2636–2641.
11 S. Chen, Y. Liu, Q. Liu and W. Peng, *IEEE Photonics Technol. Lett.*, 2016, **28**, 2195–2198.
12 K. M. Mayer, S. Lee, H. Liao, B. C. Rostro, A. Fuentes, P. T. Scully, C. L. Nehl and J. H. Hafner, *ACS Nano*, 2008, **2**, 687–692.
13 T. Endo, S. Yamamura, N. Nagatani, Y. Morita, Y. Takamura and E. Tamiya, *Sci. Technol. Adv. Mater.*, 2005, **6**, 491–500.
14 K. Fujiwara, H. Watarai, H. Itoh, E. Nakahama and N. Ogawa, *Anal. Bioanal. Chem.*, 2006, **386**, 639–644.
15 H. M. Kim, S. M. Jin, S. K. Lee, M. G. Kim and Y. B. Shin, *Sensors*, 2009, **9**, 2334–2344.
16 J. Homola, S. S. Yee and G. Gauglitz, *Sens. Actuators, B*, 1999, **54**, 3–15.
17 G. Steiner, *Anal. Bioanal. Chem.*, 2004, **379**, 328–331.
18 C. Sönnichsen, T. Franzl, T. Wilk, G. von Plessen, J. Feldmann, O. V. Wilson and P. Mulvaney, *Phys. Rev. Lett.*, 2002, **88**, 077402.
19 D. T. Moore, *Appl. Opt.*, 1980, **19**, 1035–1038.
20 F. M. Sens, C. Prünte and H. L. Kain, *Klin. Monatsbl. Augenheilkd.*, 2001, **218**, 316–322.
21 F. H. J. Koch, K. P. Luloh, A. J. Augustin, M. S. El Agha, H. Guembel, C. Ohrloff, W. S. Grizzard and S. Sinclair, *Ophthalmologica*, 1997, **211**, 283–287.
22 F. Bortoletto, C. Bonoli, P. Panizzolo and F. Mammano, *J. Microsc.*, 2011, **242**, 100–103.
23 J. Knittel, L. Schnieder, G. Buess, B. Messerschmidt and T. Possner, *Opt. Commun.*, 2001, **188**, 267–273.
24 J. K. Kim, W. M. Lee, P. Kim, M. Choi, K. Jung, S. Kim and S. H. Yun, *Nat. Protoc.*, 2012, **7**, 1456–1469.
25 G. Oh, E. Chung and S. H. Yun, *Opt. Fiber Technol.*, 2013, **19**, 760–771.
26 T. Wang, Q. Li, P. Xiao, J. Ahn, Y. E. Kim, Y. Park, M. Kim, M. Song, E. Chung, W. K. Chung, G. O. Ahn, S. Kim, P. Kim, S. J. Myung and K. H. Kim, *Opt. Express*, 2014, **22**, 12962–12970.
27 F. Wang, H. S. S. Lai, L. Liu, P. Li, H. Yu, Z. Liu, Y. Wang and W. J. Li, *Opt. Express*, 2015, **23**, 16803–16811.
28 A. Filipkowski, B. Piechal, D. Pysz, R. Stepien, J. Cimek, A. Waddie, M. Klimczak, P. Stafiej, M. R. Taghizadeh and R. Buczynski, *Photonics Lett. Pol.*, 2016, **8**, 36–38.
29 http://welcome.gofoton.com/passive-optics/selfoc-lenses/.
30 E. J. Smythe, M. D. Dickey, G. M. Whitesides and F. Capasso, *ACS Nano*, 2008, **3**, 59–65.
31 H. SadAbadi, S. Badilescu, M. Packirisamy and R. Wüthrich, *Biosens. Bioelectron.*, 2013, **44**, 77–84.
32 A. Horrer, K. Krieg, K. Freudenberger, S. Rau, L. Leidner, G. Gauglitz, D. P. Kern and M. Fleischer, *Anal. Bioanal. Chem.*, 2015, **407**, 8225–8231.

33 E. Ouellet, C. Lausted, T. Lin, C. W. T. Yang, L. Hood and E. T. Lagally, *Lab Chip*, 2010, **10**, 581–588.
34 M. M. Miller and A. A. Lazarides, *J. Phys. Chem. B*, 2005, **109**, 21556–21565.
35 S. W. Lee, K. S. Lee, J. Ahn, J. J. Lee, M. G. Kim and Y. B. Shin, *ACS Nano*, 2011, **5**, 897–904.
36 C. Schäfer, D. P. Kern and M. Fleischer, *Lab Chip*, 2015, **15**, 1066–1071.